Excited-state intramolecular proton transfer of 2-acetylindan-1,3-dione studied by ultrafast absorption and fluorescence spectroscopy

Pramod Kumar Verma,[1,a)] Andreas Steinbacher,[1] Alexander Schmiedel,[2] Patrick Nuernberger,[3] and Tobias Brixner[1,b)]

[1]*Institut für Physikalische und Theoretische Chemie, Universität Würzburg, Am Hubland, 97074 Würzburg, Germany*
[2]*Institut für Organische Chemie, Universität Würzburg, Am Hubland, 97074 Würzburg, Germany*
[3]*Physikalische Chemie II, Ruhr-Universität Bochum, 44780 Bochum, Germany*

We employ transient absorption from the deep-UV to the visible region and fluorescence upconversion to investigate the photoinduced excited-state intramolecular proton-transfer dynamics in a biologically relevant drug molecule, 2-acetylindan-1,3-dione. The molecule is a ß-diketone which in the electronic ground state exists as exocyclic enol with an intramolecular H-bond. Upon electronic excitation at 300 nm, the first excited state of the exocyclic enol is initially populated, followed by ultrafast proton transfer ($\approx$160 fs) to form the vibrationally hot endocyclic enol. Subsequently, solvent-induced vibrational relaxation takes place ($\approx$10 ps) followed by decay ($\approx$390 ps) to the corresponding ground state. *© 2015 Author(s). All article content, except where otherwise noted, is licensed under a Creative Commons Attribution 3.0 Unported License.* [http://dx.doi.org/10.1063/1.4937363]

I. INTRODUCTION

Excited-state intramolecular proton transfer (ESIPT) is one of the most successful model systems for the examination of complex proton transfer dynamics.[1–3] In a photoinduced ESIPT reaction, a proton moves from the donor to an acceptor group within the same molecule upon a change in electronic charge distribution in response to an electronic excitation. In general, ESIPT is an ultrafast process occurring on a subpicosecond time scale, but it is also reflected in spectral changes of steady-state UV/visible (VIS) absorption and fluorescence. The fluorescence emitted by the ESIPT product's excited state that is energetically much more stable than the one of the initial electronically excited reactants, not only significantly deviates from the mirror image of the absorption but is also strongly red-shifted with a Stokes shift ranging from 6000 to 10 000 cm^{-1}, as seen in the landmark work by Weller on methyl salicylate.[4,5] The origin of strongly red-shifted fluorescence spectra in these and related compounds is believed to originate from a profound rearrangement of the molecular structure, resulting from proton transfer along a pre-existing intramolecular H-bond after electronic excitation. To directly observe ESIPT in the electronically excited state, time-resolved measurements with femto- to picosecond time resolution are required. The real-time dynamics of such a proton transfer in various ESIPT molecular systems have been explored in the gas phase,[6–10] techniques applied to ESIPT in solution comprise time-resolved fluorescence based on streak cameras,[11] time-correlated single-photon counting,[12–14] and upconversion,[12,15–17] as well as transient absorption (TA) with pump/probe combinations being UV/mid-IR,[2,16,18–20] UV/VIS,[12–14,16,19–29] and recently UV/UV.[27,29] Most

a)Present address: Center for Molecular Spectroscopy and Dynamics, Institute for Basic Science (IBS), Korea University, Seoul 02841, South Korea and Department of Chemistry, Korea University, Seoul 02841, South Korea.
b)Author to whom correspondence should be addressed. Electronic mail: brixner@phys-chemie.uni-wuerzburg.de

of these ultrafast measurements have shown that ESIPT typically occurs on a subpicosecond time scale, with a key role for the low-frequency Raman-active modes modulating the H-bond distance between the proton donor and the acceptor atom.[11,25,30–38]

2-acetylindan-1,3-dione (AID) is a ß-diketone with an exocyclic double bond and has been shown to exist as exocyclic enol form (see molecular structure in Figure 1) in solution by various theoretical and experimental studies.[39–43] Apart from being a bio-active drug molecule with antibacterial and anticoagulant activities, it is a promising chelating and sunscreen agent.[44–46] Its six-membered ring structure via intramolecular H-bonding is of special interest from the viewpoint of ESIPT. Steady-state measurements of AID reveal that the fluorescence spectrum is not a mirror image and largely red-shifted compared with its absorption spectrum, suggesting ESIPT.[42] Quantum-chemical calculations support the possibility of ESIPT in AID.[42] Gaining further insight into the photochemical processes taking place in the excited state of AID necessitates time-resolved spectroscopic studies.

In this work, we combine results from fluorescence upconversion in the VIS with TA covering a broad spectral range from the deep-UV to the VIS spectral region. In contrast to the previous studies on ESIPT in other molecules, this allows not only the observation of signatures from the excited state of the involved species but also of the ground-state bleach (GSB) of the reactant. The observed dynamics are discussed in relation to ESIPT, solvation, and vibrational relaxation processes.

II. MATERIAL AND METHODS

AID (CAS No. 1133-72-8) was obtained from Sigma-Aldrich and used as received. Spectroscopic-grade solvents were also obtained from Sigma-Aldrich. The steady-state absorption and fluorescence spectra were recorded on a Jasco V670 UV-VIS and an Edinburgh Instruments FLS900 spectrometer, respectively. The wavelength-dependent sensitivity of the fluorometer was checked by comparing a measurement of Coumarin 153 with a reference spectrum from Ref. 52. For the time-resolved measurements, a fresh sample of 5×10^{-4} M concentration was prepared each time.

A detailed description of the utilized TA setup can be found elsewhere.[27] Briefly, a fraction of the fundamental beam from a commercial Ti:sapphire regenerative-amplifier laser system (Spitfire Pro, Spectra-Physics, center wavelength $\lambda_c = 800$ nm, pulse duration $\Delta\tau = 120$ fs, repetition rate $\nu_{rep} = 1$ kHz) was used to seed a commercial non-collinear optical parametric amplifier (TOPAS White, Light Conversion) which was frequency-doubled to generate the UV pump beam. Another part of the fundamental beam was used to generate the third harmonic (267 nm) which was then focused into a linearly moving 5 mm thick CaF_2 window to generate a broadband UV probe continuum ranging from 220 to 330 nm. A custom-designed spectral filter (Laser Components) was used to suppress the high spectral power around 267 nm contained within the broadband UV probe beam, which also caused unwanted reduction in the absorption intensity around 267 ± 8 nm. For the VIS probe continuum, the fundamental beam, rather than the third harmonic, of the amplifier system was focused into the moving CaF_2. Pump and probe were focused in a nearly collinear geometry at the sample position with magic-angle configuration for the linear polarization directions.[47] After passing through the sample, the probe beam was spectrally resolved via a spectrograph (Acton SP2500i) equipped with a CCD camera (Princeton Instruments Pixis 2 k). The detection was performed on a shot-to-shot basis, i.e., a mechanical chopper was utilized to block every other pump pulse. Thus, consecutive probe signals were recorded to acquire pump-induced changes in the absorbance of the sample. The analysis of the TA maps, consisting of a three-dimensional dataset (wavelength, pump–probe delay, and absorbance change), was performed with the help of the software GloTarAn, which also accounts for instrument response function (IRF), dispersion, and coherent artifact during the fitting process.[48–50] TA measurements were also performed with the neat solvents only. Pump-induced signals arising purely from the solvents were found to be negligible.[27,29]

For the fluorescence upconversion measurement, a commercial setup (Halcyone, Ultrafast Systems) was used with the details provided elsewhere.[51] Briefly, part of the fundamental beam

of another amplified Ti:Sapphire laser (Solstice, Spectra-Physics, $\lambda_c = 800$ nm, $\Delta\tau = 100$ fs, $\nu_{rep} = 1$ kHz) was used to pump an optical parametric amplifier (TOPAS, Light Conversion) to generate the UV pump beam centered at 300 nm. The fluorescence collected from the sample was focused on a 0.5-mm β-barium borate (BBO) crystal for type-I frequency upconversion with another part of the fundamental beam acting as gate pulse. The gate pulse was time-delayed with respect to the fluorescence using a motorized optical delay line. The upconverted light was focused onto the entrance slit of a double monochromator and detected by a photo-multiplier tube. The instrument response was estimated to be 350 fs by measuring stray light or Raman signals of the neat solvents.[51] The femtosecond fluorescence decays were deconvoluted globally (with OriginPro 2015 software) using a Gaussian-shaped IRF (fixed at 350 fs) and a multi-exponential function, $I(\lambda, t) = \sum_i \alpha_i(\lambda) \exp\left[-t/\tau_i(\lambda)\right]$, where $\alpha_i(\lambda)$ are pre-exponential factors, $\tau_i(\lambda)$ are the decay times, and $\sum \alpha_i(\lambda) = 1$. Next, we computed a new set of intensity decays, normalized so that the time-integrated intensity at each wavelength was equal to the steady-state intensity at that wavelength.[52] The equation used was

$$I'(\lambda, t) = H(\lambda)I(\lambda, t) = \left[\frac{I_{ss}(\lambda)}{\sum_i \alpha_i(\lambda)\tau_i(\lambda)}\right]I(\lambda, t) = \sum_i \alpha_i'(\lambda)\exp\left[-t/\tau_i(\lambda)\right], \qquad (1)$$

where $I_{ss}(\lambda)$ is the steady-state emission spectrum and $\alpha_i'(\lambda) = H(\lambda)\alpha_i(\lambda)$.[52] The values of $I'(\lambda, t)$ were used to calculate the intensity at any wavelength and time, and thus the time-resolved emission spectra (TRES). The use of Eq. (1) is well-suited when the fluorescence signal decays to zero signal within the measured time window. The TRES were fitted to a log-normal line-shape function[53] as available in OriginPro 2015 software.

III. RESULTS

Figure 1 shows the linear electronic absorption (solid) and emission spectra (dashed) of AID in hexane and acetonitrile. The electronic absorption spectrum consists of two bands in the region of 260–330 nm. The long-wavelength side exhibits a well-defined vibrational structure with two maxima of almost equal intensity peaking at 299 and 309 nm in hexane. The peaks undergo $\approx$2 nm red shifts on changing the solvent from non-polar (hexane) to polar (acetonitrile). The position of the other absorption maximum is negligibly dependent on the solvent polarity. On excitation with 300 nm light, fluorescence emission starting from 440 nm is observed peaking at 520 and 535 nm in hexane and acetonitrile, respectively. The fluorescence spectra are broad, structureless, and lack mirror symmetry with the longest-wavelength
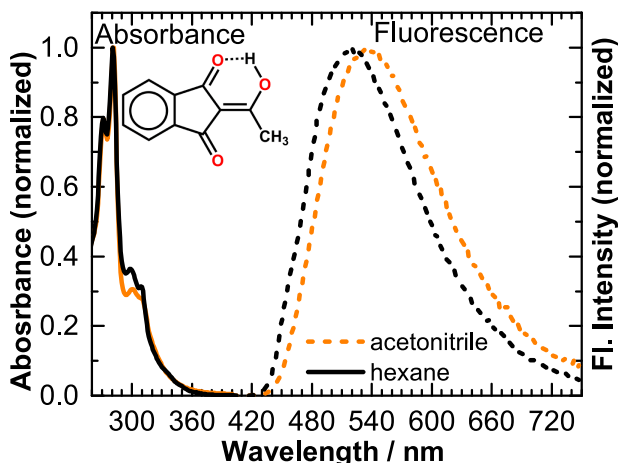

FIG. 1. The absorption (solid) and emission spectra (dashed, excitation wavelength 300 nm) of AID in hexane (black) and acetonitrile (orange). The absorption originates from AID molecules in the displayed tautomeric form.
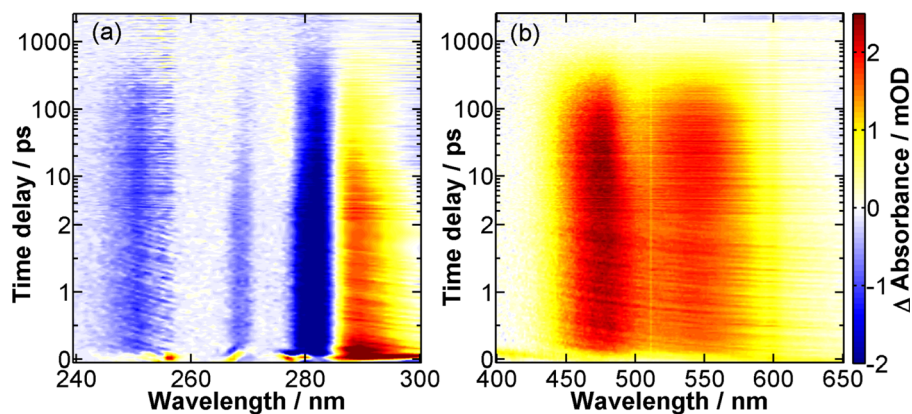
FIG. 2. Chirp-corrected TA maps of AID in acetonitrile after excitation with 300 nm pulses probed in the deep-UV (a) and in the near-UV and VIS spectral regions (b). The "uneven" ΔAbsorbance (mOD) between 260 and 275 nm is due to the characteristic of the utilized spectral filter (see Sec. II). The time delay is plotted on a linear scale up to 2 ps followed by a logarithmic scale.

absorption band. In addition, there is a large Stokes shift of $\approx 13\,000\,cm^{-1}$ (calculated from the longest-wavelength absorption band and the fluorescence maximum). These changes in the linear spectra suggest a significant geometry change of the initially electronically excited molecule preceding emission caused by ESIPT. Like the longest-wavelength absorption band, the fluorescence maximum also shifts to the red upon increase of the solvent polarity.

To get a conclusive picture of the excited-state processes that set in after absorption of UV light (300 nm) in AID, we recorded TA of AID in acetonitrile covering from the deep-UV to the VIS spectral region (Figure 2). The time evolution can be divided into three different regions. The negative signal (blue) covering the spectral region of 240–285 nm corresponds to the GSB population. The other two spectral regions give rise to positive signals (yellow/red) around 285–300 nm and 430–610 nm and are due to the excited-state absorption (ESA) from the excited species, as will be discussed below.

Figure 3 shows corresponding kinetic traces at five probe wavelengths from the three regions mentioned above. At 282 nm, GSB is observed right after excitation which recovers on a time scale of hundreds of picoseconds. At 290 nm, an ESA signal initially undergoes an
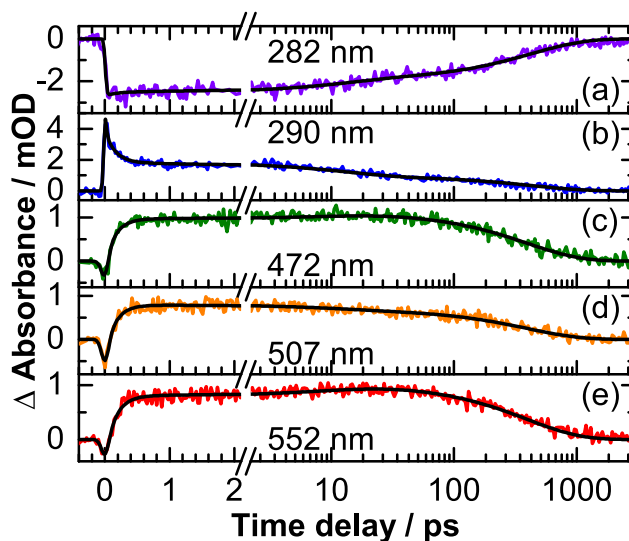

FIG. 3. Kinetic traces at selected wavelengths reflecting the excited-state dynamics of AID in acetonitrile. Results from the global fitting are shown in black. The time delay is plotted on a linear scale up to 2 ps followed by a logarithmic scale.

TABLE I. Time components obtained by global fitting of the TA data of AID in acetonitrile.

Solvent	τ_1 (fs)	τ_2 (ps)	τ_3 (ps)
TA map from Fig. 2(a)—deep-UV probe			
Acetonitrile	162 ± 6	12.9 ± 0.4	423 ± 7
TA map from Fig. 2(b)—near-UV/VIS probe			
Acetonitrile	155 ± 4	10.7 ± 0.4	394 ± 2

ultrafast decay ($\approx$160 fs) followed by a slow decay. The kinetic traces at 472, 507, and 552 nm all exhibit a rise with $\approx$160 fs followed by another small-amplitude rise on a few-picoseconds time scale and a subsequent decay ($\approx$390 ps). The ultrafast decay of ESA in the deep-UV (285–300 nm) nearly matches the observed rise of ESA in the VIS (430–610 nm). Such a decay and rise behavior resembles a typical ESIPT adiabatic cycle where the only growing step in the excited-state is the formation of the ESIPT product from the initially excited reactant. The time constants obtained from the global analysis are summarized in Table I.

To determine whether the transient absorption signal observed in the VIS domain contains contributions from stimulated emission (SE) and to determine the excited-state lifetime, time-resolved fluorescence measurements were carried out. Fluorescence upconversion signals were measured in acetonitrile for the wavelength range from 470 to 580 nm with the excitation wavelength set to 300 nm. Four exponential components were found to be sufficient for the global fitting [Table II and Figure 4(a)] of the fluorescence intensity decays at all wavelengths for AID in acetonitrile while in hexane, only three exponential components were required (Table II and Figure 5). The fluorescence decay for each wavelength has an ultrafast rise component

TABLE II. Time components obtained by global fitting of the fluorescence upconversion data of AID in acetonitrile and hexane.[a]

	Acetonitrile			
Wavelength (nm)	Amplitude of τ_1 (0.25 ± 0.01 ps)	Amplitude of τ_2 (0.60 ± 0.03 ps)	Amplitude of τ_3 (11.0 ± 0.2 ps)	Amplitude of τ_4 (383 ± 3 ps)
470	−0.62	0.92	0.36	0.34
480	−0.85	0.92	0.20	0.73
490	−1.22	1.01	0.10	1.11
500	−1.06	0.79	−0.01	1.29
510	−0.95	0.67	−0.14	1.42
520	−0.90	0.49	−0.23	1.64
530	−1.32	0.39	−0.35	2.28
540	−1.80	0.28	−0.52	3.03
550	−1.20	0.51	−0.39	2.08
560	−1.45	0.42	−0.42	2.45
570	−1.70	0.39	−0.51	2.83
580	−2.12	0.49	−0.53	3.16

	Hexane			
Wavelength (nm)	Amplitude of τ_1 (0.20 ± 0.01 ps)	Amplitude of τ_2 (-)	Amplitude of τ_3 (7.6 ± 0.33 ps)	Amplitude of τ_4 (408 ± 3 ps)
470	−0.01	—	0.10	0.91
500	−1.53	—	−0.62	3.15
570	−3.70	—	−0.81	5.51

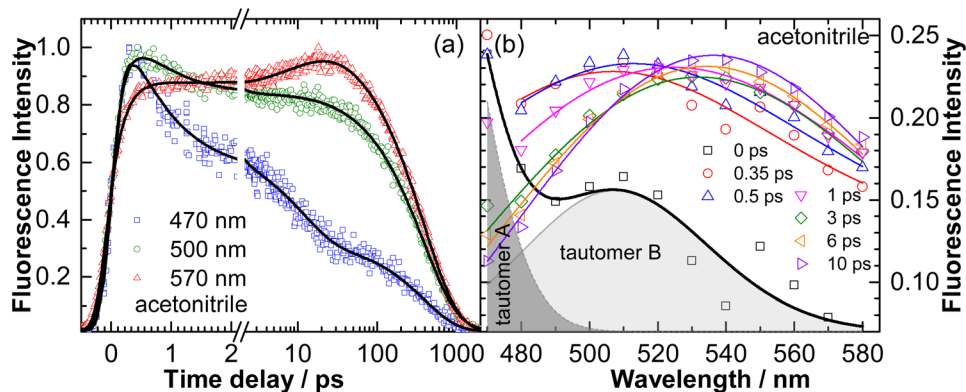[a]Negative amplitude (α_i) means rise and $\sum \alpha_i = 1$.

FIG. 4. Normalized fluorescence upconversion signal (300 nm excitation) from AID in acetonitrile at selected wavelengths (a). Reconstructed time-resolved emission spectra (TRES) of AID in acetonitrile (b). The symbols are the experimental data and the solid lines are fitting functions.

(τ_1). Though the determined value for τ_1 is close to the time resolution of the instrument (IRF: 350 fs), it is needed in the global fitting, otherwise the fitting is poor for early delay times (up to $\approx$500 fs). The decay times τ_2 and τ_3 are connected to a spectral shift, which can be described satisfactorily by a sum of exponentials.[17,19,53] The fourth component (τ_4) represents the excited-state lifetime.

The best fitted curves for three kinetic traces at wavelengths from the blue edge (470 nm), center region (500 nm), and red edge (570 nm) of the AID fluorescence spectrum are shown in Figure 4(a) along with the result of the global fit. Although the fluorescence appears instantaneously after photoexcitation at all the observed wavelengths, the subsequent dynamics vary significantly. At all wavelengths, a rising component of 0.25 (τ_1) ps is observed, which represents ESIPT. At lower wavelengths, the fluorescence exhibits a fast decay ($\tau_2 < 1$ ps) whose amplitude first increases slightly followed by subsequent decrease in amplitude with increasing wavelength. The relatively slower time component ($\tau_3 \approx 10$ ps), which first appears as decay at the blue edge, becomes a rising component at the red edge. At a time scale beyond 10 ps, the fluorescence at all wavelengths exhibits a mono-exponential decay with a time constant of $\tau_3 \approx$ 390 ps, reflecting the lifetime of the emitting excited-state of AID.

The reconstructed TRES are shown in Figure 4(b). Both the tautomer A and B exist right after excitation because the reconstructed TRES can be fitted well with a log-normal function having two peaks one centered at 453 nm [dark grey color in Figure 4(b)] and the other at
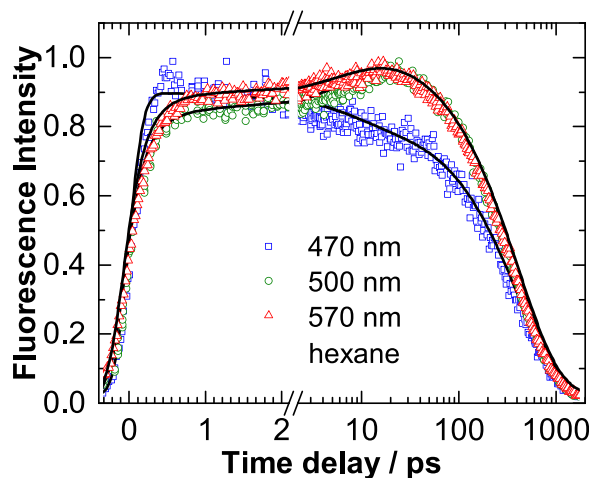

FIG. 5. Normalized fluorescence upconversion signal (300 nm excitation) from AID in hexane at selected wavelengths. The symbols are the experimental data and the solid lines are fitting functions.

509 nm [light grey color in Figure 4(b)]. Interestingly, while going from 0 ps to 0.35 ps, not only there is an increase in the intensity (area) of the tautomer B but also the TRES fitting just requires a single peak log-normal function from then on. The emission maximum undergoes a continuous red-shift with increasing delay time up to 10 ps at which the emission maximum is close to the steady-state emission value.

In non-polar solvents like hexane where solvent-shell organization is less important (but may contribute weakly[54]), we also carried out fluorescence upconversion experiments; the corresponding data are displayed in Figure 5. There is a marked difference (Table II) between the fluorescence decay of AID in hexane compared to that in acetonitrile at 470 nm, but the decay at the red side is similar for both solvents, with only marginal differences above 500 nm.

IV. DISCUSSION

A. Accessible tautomers

In the electronic ground state (S_0), the most stable conformer is the tautomer A (S_0^A; reactant state) with exocyclic double bond (Scheme 1), in agreement with experimental results and calculations.[39–43] Therefore, other rotamers are not considered as reactants, as they have not been spectroscopically observed in solution at room temperature. However, in the excited state (S_1), this is no longer the case, with tautomer B (S_1^B; ESIPT product state) being lower than S_1^A by 85.39 kJ/mol (7138 cm^{-1}).[42] This inversion of the energy order of the two tautomers in the S_1 state compared with S_0 initiates ESIPT. Enchev and co-workers[42] further showed that the S_1 state exhibits a much lower potential barrier (16.86 kJ/mol) for A → B conversion compared with the barrier (72.80 kJ/mol) in S_0 state for B → A conversion and vibrational analysis confirmed that tautomers A and B are the true minima in the S_0 and S_1 state and that the transition state in both ground and first excited electronic states has only one imaginary frequency[55] corresponding to the proton transfer coordinate. Their AM1 calculations[42] also identified an increase of 3.31 D in the dipole moment during the ESIPT reaction (S_1^A to S_1^B) which is consistent with the small shift of the emission maxima of AID from non-polar (hexane) to polar (acetonitrile) solvent (confer Figure 1). Note that there are also molecules exhibiting ESIPT where the emission blue-shifts with increasing polarity, indicating a reduction of the dipole moment when going to the excited product state.[12]

Based on spectroscopic data and the available quantum-chemical calculations, the excited-state processes in AID can be summarized as follows. The electronic excitation of AID promotes
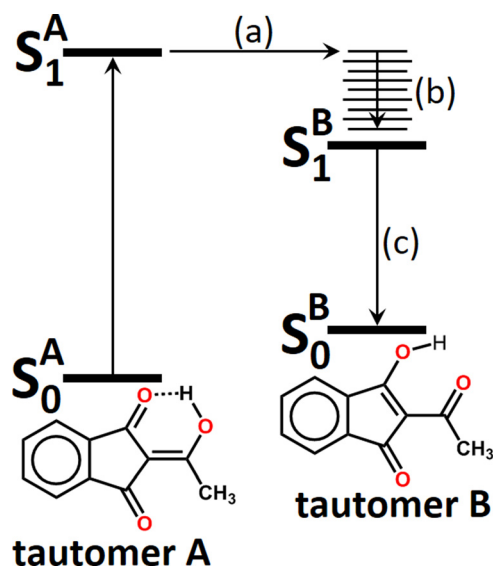
SCHEME 1. An illustrative energy diagram connecting the key steps of the photoinduced processes of AID upon electronic excitation.

the tautomer A to S_1^A via a vertical transition, subsequent rapid charge distribution results in an electronic potential surface possessing a slope, albeit with a small barrier,[42] and an energy minimum shifted towards the proton position in the tautomer B. This redistribution displaces some of the normal modes of the molecule from their equilibrium positions, which are determined by the new potential surface. As a result, the excited system moves on S_1 toward the new equilibrium position. Once the redistribution is over (expectedly occurring on a time scale below 100 fs), the low-frequency, large-amplitude modes (e.g., either in- or out-of-plane motions of the skeletal modes) change the relative position of atoms associated with the H-bond and hence channel into the proton transfer process.[25,56] Note that the excitation energy (300 nm; $33\,333\,cm^{-1}$) used in the present study is close to the onset of the AID ($S_1 \rightarrow S_0$) transition and hence it is likely that the lowest energy level of the tautomer A is directly excited.

B. Signatures of S_1^A and of ESIPT

Depending on the solvent, fluorescence spectra comprise contributions from both S_1^A and S_1^B, giving rise to "dual" fluorescence.[19] Since ESIPT is ultrafast, emission yields from the excited reactant state however may be very low (see, e.g., in Ref. 12 where the emission yield is in the order of 10^{-5}–10^{-6} for 10-hydroxybenzo[h]quinolone). Nevertheless, the observation of a corresponding emission lasting only until ESIPT is complete has been reported for different molecules.[17,23] The fitting of the TRES (Figure 4(b), dark grey area) recognizes such a weak emission of tautomer A (only a tail of the complete spectrum). Such a dual fluorescence right after excitation in molecules undergoing either intra- or intermolecular proton transfer has been reported earlier.[17,57]

Due to the continuum probing both in the deep-UV and the VIS, we have access to two other signals evidencing how fast S_1^A is depopulated. The ultrafast ESA decay in the deep-UV region [Figure 3(b)] and the ultrafast ESA rise in the VIS [Figures 3(c)–3(e)] are associated with absorptions from S_1^A and S_1^B, respectively. Thus, the proton transfer time based on our TA measurement is close to ≈160 fs (process "a" in Scheme 1) for AID which is similar to the proton transfer rates of related ESIPT molecular systems.[12,14,16,23] Our fluorescence upconversion measurement also recognizes such an ultrafast ESIPT signature, however, the determined time constant τ_1 (ESIPT) is smaller than our time resolution.

C. Solvent reorganization

The time-dependent spectral shift can arise from solvation and vibronic relaxation.[53,58] In low-viscosity polar solvents, the solvent-shell reorganization has been observed on a subpicosecond time scale, e.g., for Coumarin 153, which is complete within 1 ps in acetonitrile.[53] The time-dependent shift in the TRES clearly indicates that solvation contributes to the early excited-state processes. The time constant τ_2 determined for the fluorescence in acetonitrile, whose amplitude first increases slightly followed by subsequent decrease with increasing wavelength, might therefore be assigned to solvent reorganization. The absence of such a shift in the non-polar solvent hexane (Figure 5 and Table II) corroborates this assignment.

D. Vibrational relaxation

The occurrence of ESIPT along a highly unsymmetrical, exergonic potential energy surface should result in a highly vibrationally excited tautomer B. Since the tautomer B is higher in energy than the tautomer A by 33.68 kJ/mol ($2815\,cm^{-1}$) in the S_0 state[42] and knowing the S_0-S_1 energy gap of tautomers A and B from the absorption (311 nm; $32\,154\,cm^{-1}$) and fluorescence maxima (535 nm; $18\,691\,cm^{-1}$), the zero-point energy of the tautomer A in the S_1 state should be ≈$10\,650\,cm^{-1}$ above that of tautomer B in the S_1 state. Hence, ESIPT should provide ≈$10\,000\,cm^{-1}$ of excess energy in S_1^B. The intermediate time component of $\tau_2 \approx 10$ ps (process "b" in Scheme 1) observed in TA can be ascribed to the vibrational relaxation process of the vibrationally hot tautomer B which is also manifested in the fluorescence measurement. Vibrational relaxation comprises intramolecular vibrational relaxation (IVR; vibrational

redistribution) and intermolecular vibrational relaxation (vibrational cooling), with the former being faster than the latter.[58,59] Characteristic time scales for vibrational cooling are consistent with our measured $\approx$10 ps vibrational relaxation time.[12,17,58,60,61] Moreover, this small-amplitude rise component of $\approx$10 ps was present in both non-polar (hexane) and polar (acetonitrile) solvents, so that vibrational cooling rather than solvation gives rise to these dynamics.

E. Lifetime of S_1^B

TA data can contain various overlapping signals, both with negative sign as GSB and SE, and positive sign as ESA and absorption from product molecules. Our fluorescence upconversion measurements confirm that the longest lifetime found in the TA corresponds to an excited-state and not to a ground-state product, because the lifetimes found in TA and fluorescence upconversion are basically identical. Hence, the $S_1^B \rightarrow S_0^B$ transition (process "c" in Scheme 1) proceeds with a time constant of $\approx$390 ps.

Since fluorescence from S_1^B is observable, a corresponding SE signal should be present in the TA data. The TA data in the VIS region (Figure 2, right panel) resemble two positive peaks with identical temporal behavior, but this double-peak appearance actually is a consequence of a broad ESA signal (positive) and a weak SE (negative) right in the center, consistent with the fluorescence spectrum. Hence, the minimum in intensity near 520 nm in Figure 2 is due to overlap of weak SE (quantum yield of AID is very low $\approx$0.01)[42] with comparatively strong ESA, so that in sum only a positive signal is observed. Noteworthy, this behavior of a broad ESA modulated by a weak SE has been observed in a variety of ESIPT systems.[14,24]

F. Lifetime of S_0^B

When the emission has occurred, the product ground state S_0^B is reached, and hence the full cycle displayed in Scheme 1 is not yet complete. According to calculations,[42,46] there is also a ground-state barrier that has to be overcome to get from S_0^B to S_0^A. The TA data with deep-UV probing provide insight into the ground-state processes, because we can directly monitor the GSB of tautomer A [Figure 3(a)], which is refilled on the same time scale observed for the emission decay. Excluding the rather unlikely case that tautomers A and B have identical absorption spectra, this shows that the rate-limiting step for the full cycle is the $S_1^B \rightarrow S_0^B$ transition rather than the $S_0^B \rightarrow S_0^A$ relaxation. Hence, within less than 1 ns, the excited molecules have returned to their initial structure, i.e., tautomer A.

V. CONCLUSION

This work quantifies the steps involved in the ultrafast ESIPT reaction of the molecule AID in the condensed phase. UV excitation of AID initiates ESIPT from the tautomer A to tautomer B which occurs with a time constant of $\approx$160 fs. The tautomer B thus prepared undergoes vibrational relaxation in the order of $\approx$10 ps along the exergonic potential energy surface in the excited state. Subsequently, the thermalized tautomer B relaxes to its corresponding ground state with a time constant of $\approx$390 ps. The ground-state tautomer B then quickly turns into tautomer A. The data are well described with such a simple four-state model as shown in Scheme 1, with the characteristic time scales for the involved processes derived from TA and fluorescence upconversion measurements. The broadband TA measurements, covering also the deep-UV region, directly reveal when the full ESIPT cycle is complete.

[1] J. Goodman and L. E. Brus, J. Am. Chem. Soc. **100**, 7472–7474 (1978).

[2] T. Elsaesser and W. Kaiser, Chem. Phys. Lett. **128**, 231–237 (1986).

[3] A. Douhal, F. Lahmani, and A. H. Zewail, Chem. Phys. **207**, 477–498 (1996).

[4] A. Weller, Z. Elektrochem. **60**, 1144–1147 (1956).

[5] A. Weller, J. React. Kinet. Mech. **1**, 187–213 (1961).

[6] P. M. Felker, W. R. Lambert, and A. H. Zewail, J. Chem. Phys. **77**, 1603–1605 (1982).

[7] J. L. Herek, S. Pedersen, L. Bañares, and A. H. Zewail, J. Chem. Phys. **97**, 9046–9061 (1992).

[8] C. Lu, R.-M. R. Hsieh, I. R. Lee, and P.-Y. Cheng, Chem. Phys. Lett. **310**, 103–110 (1999).

[9] R. Srinivasan, J. S. Feenstra, S. T. Park, S. Xu, and A. H. Zewail, J. Am. Chem. Soc. **126**, 2266–2267 (2004).

[10] M. Sliwa *et al.*, Photochem. Photobiol. Sci. **9**, 661–669 (2010).

[11] P. F. Barbara, L. E. Brus, and P. M. Rentzepis, J. Am. Chem. Soc. **102**, 5631–5635 (1980).

[12] P.-T. Chou, Y.-C. Chen, W.-S. Yu, Y.-H. Chou, C.-Y. Wei, and Y.-M. Cheng, J. Phys. Chem. A **105**, 1731–1740 (2001).

[13] J. R. Choi, S. C. Jeoung, and D. W. Cho, Bull. Korean Chem. Soc. **24**, 1675–1679 (2003).

[14] S. Mitra, N. Tamai, and S. Mukherjee, J. Photochem. Photobiol. A **178**, 76–82 (2006).

[15] R. Adhikary, P. Mukherjee, T. W. Kee, and J. W. Petrich, J. Phys. Chem. B **113**, 5255–5261 (2009).

[16] O. F. Mohammed, D. Xiao, V. S. Batista, and E. T. J. Nibbering, J. Phys. Chem. A **118**, 3090–3099 (2014).

[17] S. Y. Arzhantsev, S. Takeuchi, and T. Tahara, Chem. Phys. Lett. **330**, 83–90 (2000).

[18] E. T. J. Nibbering, H. Fidder, and E. Pines, Annu. Rev. Phys. Chem. **56**, 337–367 (2005).

[19] K. Chevalier, A. Grün, A. Stamm, Y. Schmitt, M. Gerhards, and R. Diller, J. Phys. Chem. A **117**, 11233–11245 (2013).

[20] L. A. Baker, M. D. Horbury, S. E. Greenough, P. M. Coulter, T. N. V. Karsili, G. M. Roberts, A. J. Orr-Ewing, M. N. R. Ashfold, and V. G. Stavros, J. Phys. Chem. Lett. **6**, 1363–1368 (2015).

[21] T. Arthen-Engeland, T. Bultmann, N. P. Ernsting, M. A. Rodriguez, and W. Thiel, Chem. Phys. **163**, 43–53 (1992).

[22] S. Lochbrunner, A. J. Wurzer, and E. Riedle, J. Chem. Phys. **112**, 10699–10702 (2000).

[23] N. P. Ernsting, S. A. Kovalenko, T. Senyushkina, J. Saam, and V. Farztdinov, J. Phys. Chem. A **105**, 3443–3453 (2001).

[24] S. Ameer-Beg, S. M. Ormson, R. G. Brown, P. Matousek, M. Towrie, E. T. J. Nibbering, P. Foggi, and F. V. R. Neuwahl, J. Phys. Chem. A **105**, 3709–3718 (2001).

[25] S. Lochbrunner, A. J. Wurzer, and E. Riedle, J. Phys. Chem. A **107**, 10580–10590 (2003).

[26] M. Barbatti, A. J. A. Aquino, H. Lischka, C. Schriever, S. Lochbrunner, and E. Riedle, Phys. Chem. Chem. Phys. **11**, 1406–1415 (2009).

[27] P. K. Verma, F. Koch, A. Steinbacher, P. Nuernberger, and T. Brixner, J. Am. Chem. Soc. **136**, 14981–14989 (2014).

[28] L. A. Baker, M. D. Horbury, S. E. Greenough, M. N. R. Ashfold, and V. G. Stavros, Photochem. Photobiol. Sci. **14**, 1814–1820 (2015).

[29] P. K. Verma, A. Steinbacher, F. Koch, P. Nuernberger, and T. Brixner, Phys. Chem. Chem. Phys. **17**, 8459–8466 (2015).

[30] K. K. Smith and K. J. Kaufmann, J. Phys. Chem. **82**, 2286–2291 (1978).

[31] G. Weber and F. J. Farris, Biochemistry **18**, 3075–3078 (1979).

[32] J. Catalan, F. Toribio, and A. U. Acuna, J. Phys. Chem. **86**, 303–306 (1982).

[33] B. J. Schwartz, L. A. Peteanu, and C. B. Harris, J. Phys. Chem. **96**, 3591–3598 (1992).

[34] T. Fournier, S. Pommeret, J. C. Mialocq, A. Deflandre, and R. Rozot, Chem. Phys. Lett. **325**, 171–175 (2000).

[35] A. S. Klymchenko and A. P. Demchenko, Phys. Chem. Chem. Phys. **5**, 461–468 (2003).

[36] M. D. Bilokin, V. V. Shvadchak, D. A. Yushchenko, A. S. Klymchenko, G. Duportail, Y. Mely, and V. G. Pivovarenko, Tetrahedron Lett. **50**, 4714–4719 (2009).

[37] H. S. Jung, H. J. Kim, J. Vicens, and J. S. Kim, Tetrahedron Lett. **50**, 983–987 (2009).

[38] J. Kim, W. Heo, and T. Joo, J. Phys. Chem. B **119**, 2620–2627 (2015).

[39] J. D. Korp, I. Bernal, and T. L. Lemke, Acta Crystallogr., Sect. B: Struct. Sci. **36**, 428–434 (1980).

[40] M. V. Petrova, E. E. Liepins, J. J. Paulins, I. Y. Gudele, and E. Y. Gudriniece, Izv. Acad. Nauk Latv. SSR, Ser. Khim. **1**, 601–609 (1987).

[41] E. Liepiņš, M. V. Petrova, E. Gudriniece, J. Pauliņš, and S. L. Kuznetsov, Magn. Reson. Chem. **27**, 907–915 (1989).

[42] V. Enchev, S. Bakalova, G. Ivanova, and N. Stoyanov, Chem. Phys. Lett. **314**, 234–238 (1999).

[43] S. Angelova, V. Enchev, K. Kostova, M. Rogojerov, and G. Ivanova, J. Phys. Chem. A **111**, 9901–9913 (2007).

[44] C. H. Hassal, Experientia **6**, 462–464 (1950).

[45] J. T. Correll, L. L. Coleman, S. Long, and R. F. Willy, Exp. Biol. Med. **80**, 139–143 (1952).

[46] A. Ahmedova, V. Mantareva, V. Enchev, and M. Mitewa, Int. J. Cosmet. Sci. **24**, 103–110 (2002).

[47] S. Schott, A. Steinbacher, J. Buback, P. Nuernberger, and T. Brixner, J. Phys. B **47**, 124014 (2014).

[48] I. H. M. van Stokkum, D. S. Larsen, and R. van Grondelle, Biochim. Biophys. Acta, Bioenerg. **1657**, 82–104 (2004).

[49] K. M. Mullen and I. H. M. V. Stokkum, J. Stat. Software **18**, 1–46 (2007).

[50] J. J. Snellenburg, S. Laptenok, R. Seger, K. M. Mullen, and I. H. M. v. Stokkum, J. Stat. Software **49**, 1–22 (2012).

[51] F. Zieschang, A. Schmiedel, M. Holzapfel, K. Ansorg, B. Engels, and C. Lambert, J. Phys. Chem. C **117**, 19816–19831 (2013).

[52] J. R. Lakowicz, *Principles of Fluorescence Spectroscopy* (Springer US, New York, 2007), pp. 241–242.

[53] M. L. Horng, J. A. Gardecki, A. Papazyan, and M. Maroncelli, J. Phys. Chem. **99**, 17311–17337 (1995).

[54] M. Berg, J. Phys. Chem. A **102**, 17–30 (1998).

[55] T. Elsaesser and H. Van den Akker, *Ultrafast Hydrogen Bonding Dynamics and Proton Transfer Processes in the Condensed Phase* (Springer, Netherlands, 2013), p. 77.

[56] R. de Vivie–Riedle, V. De Waele, L. Kurtz, and E. Riedle, J. Phys. Chem. A **107**, 10591–10599 (2003).

[57] S. Rakshit, R. Saha, P. K. Verma, and S. K. Pal, Photochem. Photobiol. **88**, 851–859 (2012).

[58] T. Elsaesser and W. Kaiser, Annu. Rev. Phys. Chem. **42**, 83–107 (1991).

[59] N. Sarkar, S. Takeuchi, and T. Tahara, J. Phys. Chem. A **103**, 4808–4814 (1999).

[60] P. O. J. Scherer, A. Seilmeier, and W. Kaiser, J. Chem. Phys. **83**, 3948–3957 (1985).

[61] F. Laermer, T. Elsaesser, and W. Kaiser, Chem. Phys. Lett. **156**, 381–386 (1989).